

# Gentlest ascent dynamics on manifolds defined by adaptively sampled point-clouds

Juan M. Bello-Rivas,<sup>\*,†</sup> Anastasia Georgiou,<sup>†</sup> Hannes Vandecasteele,<sup>‡</sup> and Ioannis

G. Kevrekidis<sup>\*,†,¶</sup>

<sup>†</sup>*Department of Chemical and Biomolecular Engineering, Whiting School of Engineering,  
Johns Hopkins University, 3400 North Charles Street, Baltimore, 21218, MD, USA*

<sup>‡</sup>*Department of Computer Science, KU Leuven*

<sup>¶</sup>*Departments of Applied Mathematics and Statistics, Johns Hopkins University, 3400  
North Charles Street, Baltimore, 21218, MD, USA*

E-mail: jmbr@jhu.edu; yannisk@jhu.edu

## Abstract

Finding saddle points of dynamical systems is an important problem in practical applications such as the study of rare events of molecular systems. Gentlest ascent dynamics (GAD)<sup>1</sup> is one of a number of algorithms in existence that attempt to find saddle points in dynamical systems. It works by deriving a new dynamical system in which saddle points of the original system become stable equilibria. GAD has been recently generalized to the study of dynamical systems on manifolds (differential algebraic equations) described by equality constraints<sup>2</sup> and given an extrinsic formulation. In this paper, we present an extension of GAD to manifolds defined by point-clouds and formulated intrinsically. These point-clouds are adaptively sampled during an iterative process that drives the system from the initial conformation (typically in the neighborhood of a stable equilibrium) to a saddle point. Our method requires the reactant

(initial conformation), does not require the explicit constraint equations to be specified, and is purely data-driven.

## Introduction

The problem of finding saddle points of dynamical systems has one of its most notable applications in the search for transition states of chemical systems described at the atomistic level, since saddle points coincide with transition states<sup>3</sup> at the zero temperature limit. While finding local stable equilibria (sinks) is a relatively straightforward matter, finding saddle points is a more complicated endeavor for which a number of algorithms have been presented in the literature.<sup>4</sup>

Saddle point search methods can be classified according to whether they require one single input state (usually the reactant, located at the minimum of a free energy well) or two states (reactant *and* product). The Gentlest Ascent Dynamics (GAD)<sup>1</sup> belongs to the class of methods requiring a single reactant state as input and its applicability has been demonstrated with atomistic chemical systems.<sup>5,6</sup> GAD can be regarded as a variant of the dimer method that is formulated as a smooth dynamical system whose integral curves with initial condition at the reactant state can lead to saddle points. Variants of GAD such as high-index saddle dynamics (HiSD) have been the subject of recent research efforts and applications.<sup>2,7-13</sup>

While many search schemes attempt to find an optimal path between reactant and product (or between reactant state and transition state), it is interesting that there exist continuous curves joining the desired states in a variety of ways: following isoclines,<sup>14,15</sup> gradient extremals,<sup>16,17</sup> and the GAD studied in this paper. In most cases the study of these curves has been carried out in the Euclidean setting with some exceptions on the manifold of internal coordinates<sup>6,18</sup> and on manifolds defined by the zeros of smooth maps<sup>2</sup> (in these cases, the algorithms are formulated extrinsically on the ambient space). Our contribution is for-

ulated intrinsically and is valid on arbitrary manifolds, not necessarily explicitly defined by an atlas or by the zeros of maps. Algorithms like the one presented here or our previous work<sup>19</sup> do not rely on *a priori* knowledge of good collective coordinates, but rather use manifold learning to find them on the fly. In our method, there is a feedback loop of data collection that drives progress towards a saddle point.

In this paper, we study an application of the GAD to manifolds defined by point-clouds. The manifold need not be characterized in advance either by the zeros of a smooth function or an atlas, and it is only assumed that the user is capable of sampling the vicinity of arbitrary points on the manifold (*e.g.*, umbrella sampling based on reduced local coordinates). The algorithm uses dimensionality reduction (namely, diffusion map coordinates<sup>20</sup>) to define a dynamical system intrinsically on the reduced coordinates that can lead to a saddle point. Since the saddle point in general is not expected to lie in the vicinity of the reactant, our algorithm works by iteratively sampling the manifold on the fly, resolving the path on the local chart, and repeatedly switching charts until convergence. Our approach shares algorithmic elements with our previous work<sup>19</sup> which, however, instead of GAD dynamics on manifolds, was following isoclines on manifolds.

## Gentlest Ascent Dynamics and Idealized Saddle Dynamics

Gentlest Ascent Dynamics (GAD)<sup>1</sup> is an algorithm for finding saddle points of dynamical systems. We propose an extension of GAD to manifolds defined by point-clouds that finds saddle points combining nonlinear dimensionality reduction and adaptive sampling.

Let  $U: \mathbb{R}^n \rightarrow \mathbb{R}$  be a smooth potential energy function and consider the associated gradient vector field  $X$  in  $\mathbb{R}^n$  given by  $\dot{x} = X(x)$ , where  $X = -DU$  with  $D$  denoting the gradient. We restrict ourselves here, for the sake of simplicity, to the case of gradient systems and index-1 saddle points. The GAD algorithm consists of integrating the equations

of motion of the related dynamical system  $\hat{X}$  on an extended phase space  $\mathbb{R}^{2n}$  given by

$$\begin{cases} \dot{x} = H(v)(-DU)(x), \\ \dot{v} = -D^2U(x)v + r(x, v)v, \end{cases}$$

where  $H(v)w = w - (2v \cdot w)v$  is the Householder reflection<sup>21</sup> of  $w \in \mathbb{R}^n$  across the hyperplane  $\langle v \rangle^\perp = \{z \in \mathbb{R}^n \mid v \cdot z = 0\}$  and  $r(x, v) = \|v\|^{-2} v \cdot D^2U(x)v$  is the Rayleigh quotient of the Hessian matrix  $D^2U(x)$  corresponding to the vector  $v \in \mathbb{R}^n$ .

*Remark 1.* The right hand side of the ordinary differential equation for  $\dot{v}$  is the term

$$-D^2U(x)v + r(x, v)v.$$

If  $v$  is an eigenvector of  $D^2U(x)$  with eigenvalue  $\lambda$ , then  $r(x, v) = \lambda$ . Now note that the constrained optimization problem consisting of finding the extrema of  $Z(x) = \frac{1}{2}\| -DU(x) \|^2$  along the level sets  $C = \{x \in \mathbb{R}^n \mid U(x) = c\}$  is precisely given by the Lagrange equation

$$D^2U(x)DU(x) - \lambda DU(x) = 0,$$

which says that the extrema of the magnitude of the gradient,  $Z$ , along  $C$  are attained wherever the gradient field  $X = -DU$  happens to be an eigenvector of the Hessian  $D^2U$ .

## Idealized saddle-point dynamics

We consider a variant of the GAD algorithm named Idealized Saddle Dynamics (ISD),<sup>22</sup> given by

$$\dot{x} = H(x, v)(-DU)(x),$$

where  $v \in \mathbb{R}^n$  is an eigenvector of  $D^2U(x)$  corresponding to the smallest eigenvalue  $\lambda$ .

Let  $M$  be a  $d$ -dimensional smooth manifold with Riemannian metric  $g$  and let  $U \in C^\infty(M)$  be a potential energy function. We consider the gradient field  $X = -\text{grad } U \in \mathfrak{X}(M)$



and write the following equation for the ISD on  $M$ ,

$$\hat{X} = X - 2g(V, X)V \in \mathfrak{X}(M), \quad (1)$$

where  $V$  is the vector field on  $M$  defined by choosing the eigenvector (normalized so that  $g(V, V) = 1$ ) corresponding to the smallest eigenvalue of the Hessian matrix. However, in this case the Hessian must be defined in terms of the covariant derivative on  $(M, g)$  with respect to the Levi-Civita connection.<sup>23,24</sup> To be precise, given two vector fields  $S, T \in \mathfrak{X}(M)$ , we have

$$\nabla^2 U(S, T) = \nabla_T(\nabla_S U) - \nabla_{\nabla_T S} U,$$

which is a tensor of valence  $(0, 2)$ , where  $\nabla$  denotes the covariant derivative induced by the Levi-Civita connection. We apply the sharp  $(\sharp)$  isomorphism (raising or lowering indices) to turn  $\nabla^2 U$  into a  $(1, 1)$ -tensor. Therefore,

$$(\text{Hess } U)T = \nabla_T \text{grad } U.$$

The eigenvector corresponding to the lowest eigenvalue of  $\text{Hess } U$  at each point  $p \in M$  induces a vector field  $V$  whose integral curves are curves that may join an initial point with a saddle point.

The ISD formulation of GAD is particularly amenable to be coupled with dimensionality reduction approaches because the resulting eigenproblem is often of much lower dimensionality than the ambient space in which the original dynamical system is defined.

**Example 1.** Let us compute a concrete case of ISD, first with known exact formulas and later on with approximations using diffusion maps and Gaussian processes. Consider the sphere

$$\mathbb{S}^2 = \{(x^1, x^2, x^3) \in \mathbb{R}^3 \mid (x^1)^2 + (x^2)^2 + (x^3)^2 = 1\}.$$

and the stereographic projection from the North pole onto the tangent plane at the South

pole. The system of coordinates is given by

$$\phi(x^1, x^2, x^3) = \left( \frac{x^1}{1-x^3}, \frac{x^2}{1-x^3} \right) \in \mathbb{R}^2,$$

Let  $(u^1, u^2) \in \mathbb{R}^2$ . The corresponding parameterization,  $\psi = \phi^{-1}$ , is given by

$$\psi(u^1, u^2) = \frac{1}{1 + (u^1)^2 + (u^2)^2} (2u^1, 2u^2, (u^1)^2 + (u^2)^2 - 1).$$

The pullback of the Euclidean metric  $h = dx^1 \otimes dx^1 + dx^2 \otimes dx^2 + dx^3 \otimes dx^3$  by  $\psi$  gives us the metric  $g$

$$g = \psi^* h = \frac{4du^1 \otimes du^1 + 4du^2 \otimes du^2}{(1 + (u^1)^2 + (u^2)^2)^2}$$

The non-redundant Christoffel symbols  $\Gamma_{ij}^k$  that characterize the Levi-Civita connection  $\nabla$  are

$$\begin{aligned} \Gamma_{1,1}^1 &= \frac{-2u^1}{1 + (u^1)^2 + (u^2)^2}, & \Gamma_{1,2}^1 &= \frac{-2u^2}{1 + (u^1)^2 + (u^2)^2}, \\ \Gamma_{2,2}^1 &= -\Gamma_{1,1}^1, & \Gamma_{1,1}^2 &= -\Gamma_{1,2}^1, & \Gamma_{1,2}^2 &= \Gamma_{1,1}^1, & \text{and} & \Gamma_{2,2}^2 &= \Gamma_{1,2}^1. \end{aligned}$$

The energy  $E(x^1, x^2, x^3) = x^1 x^2 x^3$  defined on  $\mathbb{S}^2 \subset \mathbb{R}^3$  induces an energy  $U = \psi^* E$  on  $\mathbb{S}^2$ ,

$$U(u^1, u^2) = \frac{4u^1 u^2 ((u^1)^2 + (u^2)^2 - 1)}{((u^1)^2 + (u^2)^2 + 1)^3},$$

The force on  $\mathbb{S}^2$  is the negative of the gradient

$$\begin{aligned} \text{grad } U &= \left( \frac{(u^2)^5 - 2(u^1)^2 (u^2)^3 + (-3(u^1)^4 + 8(u^1)^2 - 1) u^2}{(u^2)^4 + (2(u^1)^2 + 2)(u^2)^2 + (u^1)^4 + 2(u^1)^2 + 1} \right) \frac{\partial}{\partial u^1} \\ &\quad + \left( -\frac{3u^1 (u^2)^4 + (2(u^1)^3 - 8u^1)(u^2)^2 - (u^1)^5 + u^1}{(u^2)^4 + (2(u^1)^2 + 2)(u^2)^2 + (u^1)^4 + 2(u^1)^2 + 1} \right) \frac{\partial}{\partial u^2} \end{aligned}$$

The potential energy and the gradient field are shown in Figure 1a.

The Hessian is then given by the  $(1, 1)$  tensor

$$\nabla \text{grad } U = A \frac{\partial}{\partial u^1} \otimes du^1 + B \frac{\partial}{\partial u^2} \otimes du^1 + B \frac{\partial}{\partial u^1} \otimes du^2 + D \frac{\partial}{\partial u^2} \otimes du^2,$$

where

$$\begin{aligned} A &= -\frac{4u^1u^2((u^2)^4 + (u^2)^2 - (u^1)^4 + 11(u^1)^2 - 6)}{((u^2)^2 + (u^1)^2 + 1)^3} \\ B &= -\frac{(u^2)^6 - 5(u^1)^2(u^2)^4 - 5(u^2)^4 - 5(u^1)^4(u^2)^2 + 30(u^1)^2(u^2)^2 - 5(u^2)^2 + (u^1)^6 - 5(u^1)^4 - 5(u^1)^2 + 1}{((u^2)^2 + (u^1)^2 + 1)^3} \\ D &= \frac{4u^1u^2((u^2)^4 - 11(u^2)^2 - (u^1)^4 - (u^1)^2 + 6)}{((u^2)^2 + (u^1)^2 + 1)^3}. \end{aligned}$$

The smallest eigenvector of  $\nabla \text{grad } U \in \Gamma(\mathfrak{X}(\mathbb{S}^2) \otimes \Lambda^1(\mathbb{S}^2))$  determines the vector field  $V \in \mathfrak{X}(\mathbb{S}^2)$  that is used in the formulation of the ISD vector field (1) and is shown in Figure 1b.

Example 1 required the knowledge of a particular system of coordinates (namely, the stereographic projection from the North pole to the tangent space at the South pole) mapping three-dimensional points on the sphere to two-dimensional coordinates; here this allows us to work with a single chart. In some settings the system of coordinates of the underlying manifold is either unknown or difficult to obtain. It is possible under those circumstances to replicate the steps in Example 1 in the absence of a system of coordinates given as a closed-form expression by resorting to manifold learning / dimensionality reduction techniques. In our case, as we shall discuss next, we use diffusion maps on points sampled from a local neighborhood of the manifold to extract a suitable system of coordinates. Fitting a Gaussian process to the diffusion map coordinates of the point-cloud yields a local system of coordinates  $\phi$  that can be evaluated at arbitrary points (not necessarily those in the sampled point-cloud). Once we have a system of coordinates, we can again proceed to estimate the Riemannian metric as well as the Levi-Civita connection, and compute the flow of the ISD vector field  $\hat{X}$  given in (1) to find saddle points.

Revisiting Example 1 and approaching it with the aforementioned procedure allows us to obtain trajectories that lead to saddle points, as shown in Figures 3 to 5.

# Algorithm

Consider the manifold  $M \subset \mathbb{R}^n$  and the gradient dynamical system  $X \in \mathfrak{X}(M)$ . We begin by drawing a total of  $N$  samples from the manifold  $M$  in the neighborhood of an initial point  $p \in M$ . This can be done in a variety of ways depending on the application. If  $M$  is the inertial manifold of a dynamical system  $X$ , then a reasonable way to approach this problem is to generate  $N$  distinct perturbations  $\{p_{(i)} \in \mathbb{R}^n \mid i = 1, \dots, N\}$  of  $p$  and propagate them according to the flow of  $X$  during a (short) time horizon  $\tau > 0$ . Doing so, we obtain a data set  $\mathcal{D} = \{q_{(i)} = \exp_\tau p_{(i)} \in M \mid i = 1, \dots, N\}$  approximately on the manifold. Alternatively, one may numerically solve a stochastic differential equation such as the Brownian dynamics equation,

$$dq_t = X(q_t) dt + \sigma dB_t, \quad (2)$$

where the drift is the vector field  $X$ ,  $\sigma > 0$  is a constant, and  $B_t$  is a standard  $n$ -dimensional Brownian motion. Solving (2) (possibly with an added RMSD-based restraint around the initial conformation) up to a certain time  $\tau > 0$  and extracting an uncorrelated subset of the states at different time steps yields a data set  $\mathcal{D} = \{q_{(i)} = q_{t_i} \mid i = 1, \dots, N, 0 \leq t_1 \leq \dots \leq t_N \leq \tau\}$ .

Next, we apply a dimensionality reduction algorithm on the data set  $\mathcal{D}$  to obtain a set of reduced coordinates  $\phi$ . In our case, we use diffusion maps<sup>20,25</sup> to obtain a set of vectors  $\phi_{(i)} \in \mathbb{R}^d$  with  $d \leq n$  but other methods, such as local tangent space alignment,<sup>26</sup> may be used as well. It is important to note that our dimensionality reduction method is applied to a local neighborhood of an initial point and, therefore, it is expected to yield a reasonable approximation to a chart on that neighborhood.

We fit a Gaussian process regressor  $\phi$  to the pairs of points  $(q_{(i)}, \phi_{(i)}) \in \mathbb{R}^n \times \mathbb{R}^d$  to obtain a smooth map  $\phi: M \subset \mathbb{R}^n \rightarrow \mathbb{R}^d$  that will act as a system of coordinates (in particular,  $\phi(q_{(i)}) \approx \phi_{(i)}$ ). Proceeding in an analogous fashion, we compute the inverse mapping  $\psi = \phi^{-1}$ .

*Remark 2.* We can reduce the computational expense of the Gaussian process regression by reusing the kernel matrix with entries  $e^{-\|q_{(i)} - q_{(j)}\|^2/2\varepsilon}$  (for some  $\varepsilon > 0$ ) calculated during the computation of the diffusion map coordinates as the covariance matrix for the Gaussian process (assuming that it is formulated using the squared exponential kernel).

*Remark 3.* It is not always possible to obtain a suitable Gaussian process regressor for  $\psi = \phi^{-1}$ . An alternative is to add an Ornstein-Uhlenbeck process to the stochastic differential equation (2) in order to obtain

$$dq_t = (X(q_t) - \kappa(\phi(q_t) - \phi_0)) dt + \sigma dB_t,$$

where  $\kappa > 0$  is a hyperparameter and  $\phi_0$  is a prescribed point not necessarily in  $\phi(\mathcal{D})$ . Computing the ensemble average  $\langle q_t \rangle$  of the solution to the above equation yields a point  $q_{(0)}$  such that  $\phi(q_{(0)}) \approx \phi_0$  or, equivalently,  $q_{(0)} = \psi^{-1}(\phi_0)$ . This works because the new term added to the drift nudges the system towards a point in ambient space such that its image by  $\phi$  is the prescribed point  $\phi_0$ .

We consider the values  $X_{q_{(i)}} \in TM$  of the vector field  $X$  at the points in the data set  $\mathcal{D}$  and map them via the system of coordinates in order to obtain  $\phi_* X_{q_{(i)}} = D\phi(q_{(i)})X_{q_{(i)}}$ , where  $D\phi$  is the Jacobian matrix of  $\phi$  (note that the Jacobian-vector product can be computed either as a closed-form formula or efficiently using automatic differentiation — *e.g.*, using `jvp` in `Jax`<sup>27</sup>).

At this stage, we can readily compute the Riemannian metric  $g$  as

$$g = \sum_{i,j=1}^d g_{ij} d\phi^i \otimes d\phi^j, \quad (3)$$

where  $g_{ij} = D\psi^\top D\psi$  for  $i, j = 1, \dots, d$ . The metric induces an inner product, denoted by the bracket  $\langle \cdot, \cdot \rangle$ , between tangent vectors such that if  $S = \sum_{i=1}^d S^i \frac{\partial}{\partial \phi^i}$  and  $T = \sum_{i=1}^d T^i \frac{\partial}{\partial \phi^i}$  are the expressions in local coordinates of two tangent vectors  $S, T \in T_u M$  at a point  $u \in M$ ,

then  $\langle S, T \rangle = \sum_{i,j=1}^d g_{ij} S^i T^j$ .

Using (3), we obtain the coefficients of the Levi-Civita connection,<sup>23</sup>

$$\Gamma_{jk}^\ell = \sum_{i=1}^d g^{\ell i} \left( \frac{\partial g_{ij}}{\partial \phi^k} + \frac{\partial g_{ik}}{\partial \phi^j} - \frac{\partial g_{jk}}{\partial \phi^i} \right)$$

for  $j, k, \ell \in \{1, \dots, d\}$ , where  $g^{ij}$  denotes the entries of the inverse of the matrix with components  $g_{ij}$ . This, in turn, allows us to take the covariant derivative and the Hessian, defined by

$$\text{Hess } U(S, T) = \langle \nabla_T \text{grad } U, S \rangle$$

for arbitrary tangent vectors  $S, T$ . Observe that the Hessian is defined on the local chart, not on the ambient space. The eigenvector  $V$ , normalized with respect to  $g$ , with smallest eigenvalue of the Hessian then yields a vector field

$$\hat{X} = X - 2Vg(V, X)$$

such that the index-1 saddle points of  $X$  become stable equilibria<sup>1</sup> of  $\hat{X}$ . Consequently, an integral curve of  $\hat{X}$  in the vicinity of a saddle point leads to the saddle point.

In general, in order to carry out the computation until convergence, we must frequently switch charts. This is due to the fact that at each step, we sample a point-cloud  $\mathcal{D}$  in a small neighborhood of a given point and the Gaussian process regressor  $\phi$  yields an approximation to  $X$  on the chart that cannot extrapolate far away from the sampled points. Therefore, when we reach the confines of  $\mathcal{D}$  (which can be determined by the density of points), we ought to map the latest point of our integral curve of  $\hat{X}$  from the chart back to the ambient space using  $\psi = \phi^{-1}$ , as discussed earlier. After that, we start the whole procedure again: sample a new data set  $\mathcal{D}$ , compute  $\phi$ , trace an integral curve of  $\hat{X}$ , etc.

*Remark 4.* An alternative approach to the one presented here could consist of exploiting the fact that GAD trajectories are geodesics<sup>28</sup> of a Finsler metric<sup>29,30</sup> and to numerically

compute said geodesics in each learned local chart in a similar manner to what we propose.

## Numerical example

The preceding algorithm applied to the vector field on the sphere  $\mathbb{S}^2$  introduced in Example 1 produces the iterations shown in Figures 3, 4, and 5. These figures depict the integral curves (highlighted) in the local neighborhoods obtained by sampling and integrating  $\hat{X}$ . The full integral curve joining the initial point to a saddle point at the equator of the sphere in Figure 2. The computations were done with the help of the JAX<sup>27</sup> and Diffrax<sup>31</sup> libraries, and the code to reproduce our results is available at [https://github.com/jmbr/gentlest\\_ascent\\_dynamics\\_on\\_manifolds](https://github.com/jmbr/gentlest_ascent_dynamics_on_manifolds).

## Conclusions

We have presented a formulation of GAD on manifolds defined by point-clouds that are meant to be sampled on-demand. Our formulation is intrinsic and does not require the specification of the manifolds either by a given atlas or by the zeros of a smooth map. The required charts are discovered through a data-driven, iterative process that only requires knowledge of an initial conformation of the reactant. We illustrated our approach with the example of a vector field on the 2-sphere and we expect the results to transfer to the high-dimensional dynamical systems of interest in computational statistical mechanics.

## Acknowledgement

This work was supported by the US Air Force Office of Scientific Research (AFOSR) and the US Department of Energy DOE with IIT: SA22-0052-S001 and AFOSR-MURI: FA9550-21-1-0317.

## References

- (1) E, W.; Zhou, X. The Gentlest Ascent Dynamics. *Nonlinearity* **2011**, *24*, 1831–1842.
- (2) Yin, J.; Huang, Z.; Zhang, L. Constrained High-Index Saddle Dynamics for the Solution Landscape with Equality Constraints. *Journal of Scientific Computing* **2022**, *91*, 62.
- (3) Hänggi, P.; Talkner, P.; Borkovec, M. Reaction-Rate Theory: Fifty Years after Kramers. *Reviews of Modern Physics* **1990**, *62*, 251–341.
- (4) Olsen, R. A.; Kroes, G. J.; Henkelman, G.; Arnaldsson, A.; Jónsson, H. Comparison of Methods for Finding Saddle Points without Knowledge of the Final States. *The Journal of Chemical Physics* **2004**, *121*, 9776–9792, Publisher: American Institute of Physics.
- (5) Samanta, A.; Chen, M.; Yu, T.-Q.; Tuckerman, M.; E, W. Sampling saddle points on a free energy surface. *The Journal of Chemical Physics* **2014**, *140*, 164109–164109.
- (6) Quapp, W.; Bofill, J. M. Locating saddle points of any index on potential energy surfaces by the generalized gentlest ascent dynamics. *Theoretical Chemistry Accounts* **2014**, *133*, 1510.
- (7) Gu, S.; Zhou, X. Multiscale gentlest ascent dynamics for saddle point in effective dynamics of slow-fast system. *Communications in Mathematical Sciences* **2017**, *15*, 2279–2302, Publisher: International Press of Boston.
- (8) Gu, S.; Zhou, X. Simplified gentlest ascent dynamics for saddle points in non-gradient systems. *Chaos: An Interdisciplinary Journal of Nonlinear Science* **2018**, *28*, 123106, Publisher: American Institute of Physics.
- (9) Yin, J.; Zhang, L.; Zhang, P. High-Index Optimization-Based Shrinking Dimer Method for Finding High-Index Saddle Points. *SIAM Journal on Scientific Computing* **2019**, *41*, A3576–A3595, Publisher: Society for Industrial and Applied Mathematics.

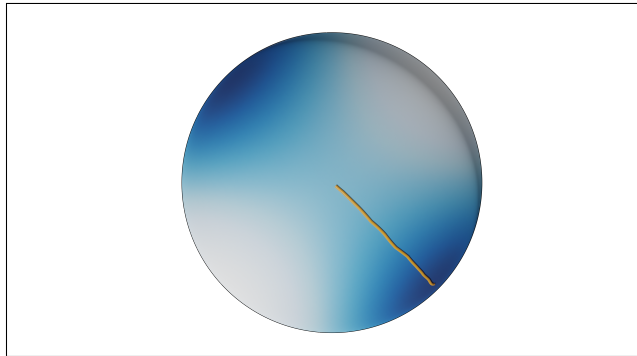


- (10) Yin, J.; Zhang, L.; Zhang, P. Solution landscape of the Onsager model identifies non-axisymmetric critical points. *Physica D: Nonlinear Phenomena* **2022**, *430*, 133081.
- (11) Gu, S.; Wang, H.; Zhou, X. Active Learning for Saddle Point Calculation. *Journal of Scientific Computing* **2022**, *93*, 78.
- (12) Luo, Y.; Zheng, X.; Cheng, X.; Zhang, L. Convergence analysis of discrete high-index saddle dynamics. 2022; <http://arxiv.org/abs/2204.00171>, arXiv:2204.00171 [cs, math].
- (13) Zhang, L.; Zhang, P.; Zheng, X. Error Estimates for Euler Discretization of High-Index Saddle Dynamics. *SIAM Journal on Numerical Analysis* **2022**, *60*, 2925–2944, Publisher: Society for Industrial and Applied Mathematics.
- (14) Quapp, W.; Hirsch, M.; Imig, O.; Heidrich, D. Searching for saddle points of potential energy surfaces by following a reduced gradient. *Journal of Computational Chemistry* **1998**, *19*, 1087–1100.
- (15) Quapp, W.; Hirsch, M.; Heidrich, D. Bifurcation of reaction pathways: the set of valley ridge inflection points of a simple three-dimensional potential energy surface. *Theoretical Chemistry Accounts* **1998**, *100*, 285–299.
- (16) Basilevsky, M. V. The topography of potential energy surfaces. *Chemical Physics* **1982**, *67*, 337–346.
- (17) Hoffman, D. K.; Nord, R. S.; Ruedenberg, K. Gradient extremals. *Theoretica chimica acta* **1986**, *69*, 265–279.
- (18) Quapp, W. Newton Trajectories in the Curvilinear Metric of Internal Coordinates. *Journal of Mathematical Chemistry* **2004**, *36*, 365–379.
- (19) Bello-Rivas, J. M.; Georgiou, A.; Guckenheimer, J.; Kevrekidis, I. G. Staying the

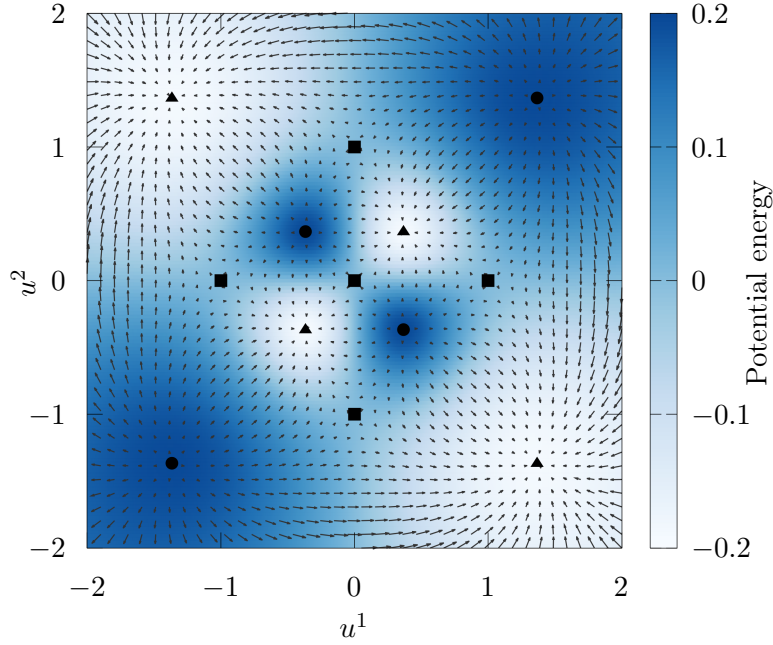
- Course: iteratively locating equilibria of dynamical systems on Riemannian manifolds defined by point-clouds. *Journal of Mathematical Chemistry* **2022**,
- (20) Coifman, R. R.; Lafon, S. Diffusion Maps. *Applied and Computational Harmonic Analysis* **2006**, *21*, 5–30.
  - (21) Golub, G. H.; Van Loan, C. F. *Matrix computations*, 4th ed.; Johns Hopkins Studies in the Mathematical Sciences; Johns Hopkins University Press: Baltimore, MD, 2013.
  - (22) Levitt, A.; Ortner, C. Convergence and Cycling in Walker-type Saddle Search Algorithms. *SIAM Journal on Numerical Analysis* **2017**, *55*, 2204–2227.
  - (23) do Carmo, M. P. *Riemannian geometry*; Mathematics: Theory & Applications; Birkhäuser Boston, Inc., Boston, MA, 1992.
  - (24) Absil, P.-A.; Mahony, R.; Sepulchre, R. *Optimization Algorithms on Matrix Manifolds*; Princeton University Press: Princeton, 2008.
  - (25) Nadler, B.; Lafon, S.; Coifman, R. R.; Kevrekidis, I. G. Diffusion maps, spectral clustering and reaction coordinates of dynamical systems. *Applied and Computational Harmonic Analysis* **2006**, *21*, 113–127.
  - (26) Zhang, Z.; Zha, H. Principal Manifolds and Nonlinear Dimensionality Reduction via Tangent Space Alignment. *SIAM Journal on Scientific Computing* **2004**, *26*, 313–338, Publisher: Society for Industrial and Applied Mathematics.
  - (27) Bradbury, J.; Frostig, R.; Hawkins, P.; Johnson, M. J.; Leary, C.; Maclaurin, D.; Necula, G.; Paszke, A.; VanderPlas, J.; Wanderman-Milne, S.; Zhang, Q. JAX: composable transformations of Python+NumPy programs. 2018; <http://github.com/google/jax>.
  - (28) Bofill, J. M.; Quapp, W. The variational nature of the gentlest ascent dynamics and the

- relation of a variational minimum of a curve and the minimum energy path. *Theoretical Chemistry Accounts* **2016**, *135*, 1–14.
- (29) Randers, G. On an Asymmetrical Metric in the Four-Space of General Relativity. *Physical Review* **1941**, *59*, 195–199.
- (30) Chern, S.-S.; Shen, Z. *Riemann-Finsler Geometry*; Nankai Tracts in Mathematics; WORLD SCIENTIFIC, 2005; Vol. 6.
- (31) Kidger, P. On Neural Differential Equations. Ph.D. thesis, University of Oxford, 2021.

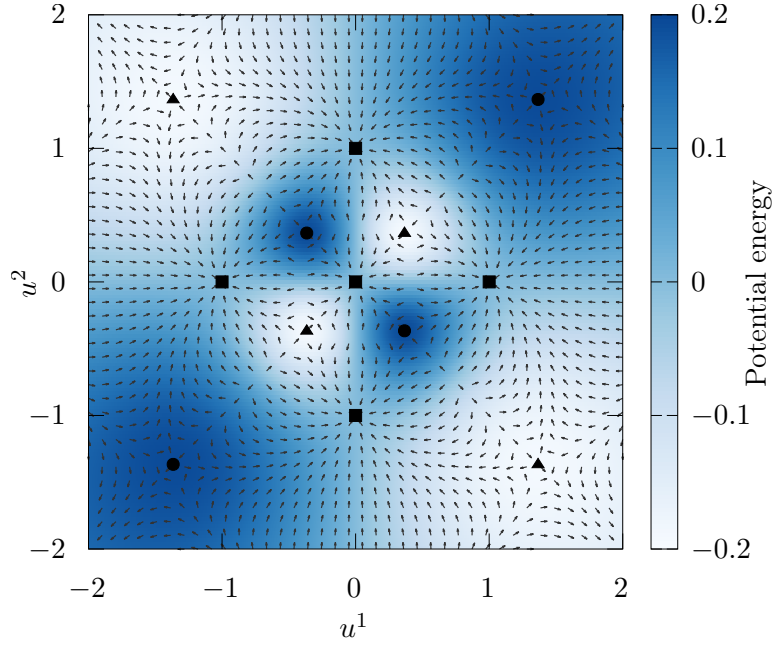
## Graphical TOC Entry



A trajectory of the saddle dynamics on a sphere computed by iteratively sampling and navigating in coordinate systems obtained on the fly via manifold learning. The trajectory starts at a sink on the lower right and reaches a saddle point at the center.



(a) Vector field corresponding to the potential energy function considered in the text.



(b) Idealized saddle dynamics vector field corresponding to the original vector field. Notice how saddle points in the original vector field become sinks (stable equilibria) of the ISD vector field.

Figure 1: Vector fields on the sphere, seen in the stereographic projection from the North pole onto the tangent plane to the South pole. The equilibria of the original vector field appear represented as  $\bullet$  for sinks,  $\blacksquare$  for saddle points, and  $\blacktriangle$  for sources.

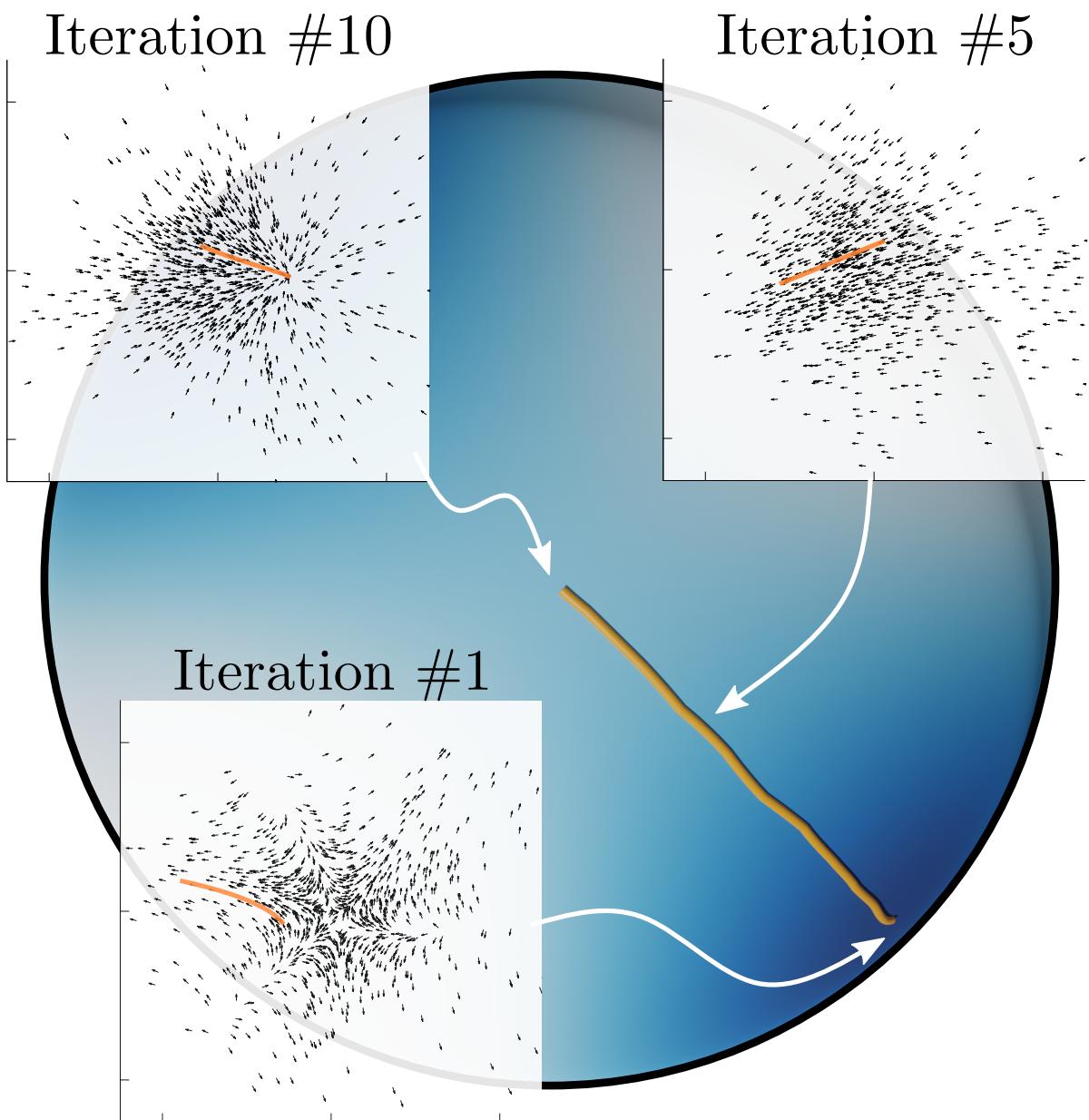


Figure 2: Resulting trajectory (in orange) of GAD/ISD on the sphere (color indicates value of the potential energy function) using diffusion maps to navigate from the sink (bottom right) to the saddle (center). The insets depict the corresponding vector fields in local coordinates at different iterations and also the GAD curve (orange). See also Figures 3, 4, and 5.

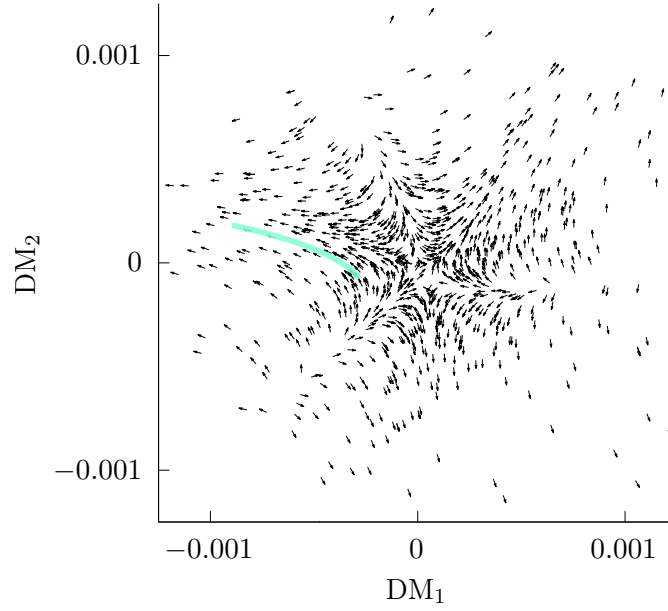


Figure 3: Iteration #1 of ISD on the sphere by sampling point-clouds and using diffusion maps. The points and the vector field are drawn from the neighborhood of a stable equilibrium. The solid curve represents the GAD/ISD path.

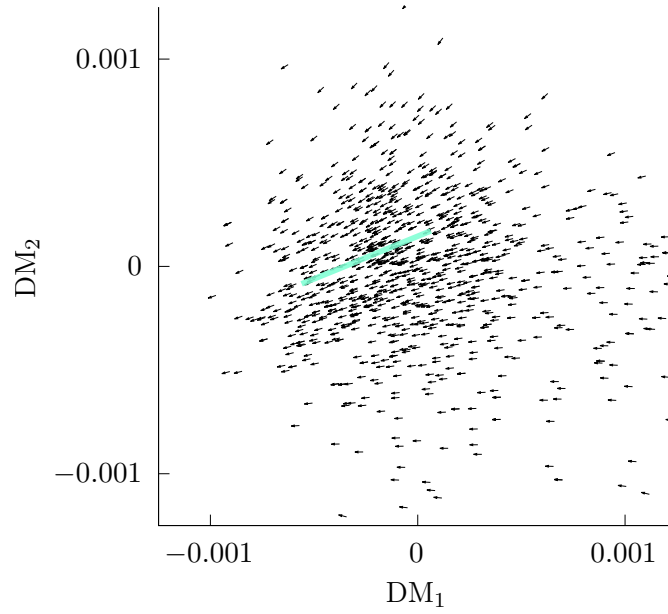


Figure 4: Iteration #5 of ISD on the sphere by sampling point-clouds and using diffusion maps.

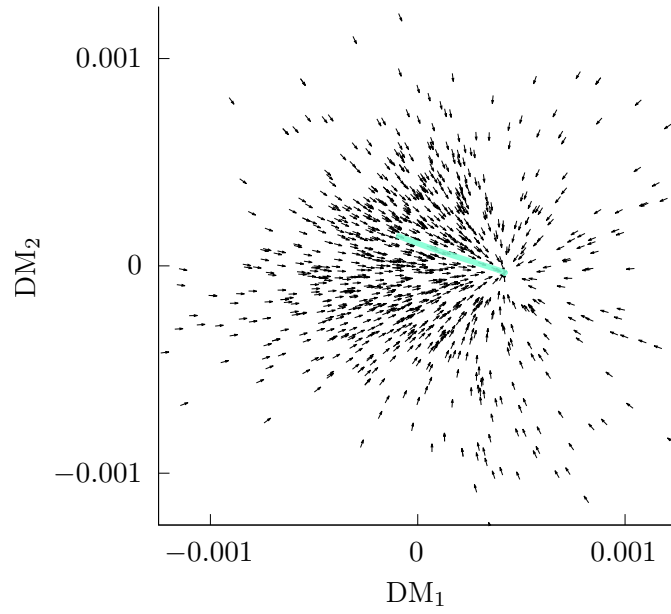


Figure 5: Iteration #10 of ISD on the sphere by sampling point-clouds and using diffusion maps. The algorithm has reached a saddle point of the original vector field (notice how it becomes a sink for the ISD vector field).